A Study of Mass Transfer Kinetics in an Enantiomeric Separation System Using a Polymeric Imprinted Stationary Phase

Kanji Miyabe and Georges Guiochon*

Department of Chemistry, The University of Tennessee, Knoxville, Tennessee 37996-1600, and Division of Chemical and Analytical Sciences, Oak Ridge National Laboratory, Oak Ridge, Tennessee 37831

Chromatographic data pertaining to the enantioseparation of L- and D-phenylalanine anilide (PA) on a polymeric stationary phase imprinted with L-PA were studied from the viewpoints of phase equilibrium, mass transfer kinetics, and the thermodynamic properties of this enantiomeric separation system. The concentration dependence of the lumped mass transfer rate coefficient ($k_{m,L}$) previously published was analyzed to obtain new information concerning the mass transfer characteristics in this chiral separation system. It was shown that intraparticle diffusion contributed much more to $k_{m,L}$ than adsorption/desorption. The positive concentration dependence of $k_{m,L}$ seemed to be interpreted by considering that of the surface diffusion coefficient, itself explained by the heterogeneous surface model. The characteristic features of the phase equilibrium, the mass transfer kinetics, and the thermodynamics of the enantiomeric separation system probably result from the adsorption energy distribution on the surface of the imprinted phase having an exponential decay.

1. Introduction

Molecular imprinted polymers are becoming popular as effective materials for functional separations. Cases in point are chiral stationary phases in chromatography and antibodies in immunoassays (Andersson, 1996; Sellergren, 1994; Sellergren and Shea, 1995; Shea et al., 1993; Vlatakis et al., 1993). Separation methods using imprinted materials are most attractive because of their high selectivity for the objective compound, the imprinted molecule. However, imprinted polymers also have major drawbacks as packing materials for chromatography. Columns packed with them exhibit low efficiency and afford unsymmetrical peaks (Sellergren, 1994; Sellergren and Shea, 1995). The poor properties of imprinted materials probably stem from the energetic heterogeneity of their surfaces and slow mass transfer kinetics inside their particles. However, Sellergren et al. (1994, 1995) suggested that these drawbacks originated from nonlinear adsorption isotherms, probably correlated with the heterogeneous energy distribution of the adsorption sites on the surface of the stationary phases (Sellergren, 1994; Sellergren et al., 1988; Sellergren and Shea, 1995). Although they also pointed out the important influence of mass transfer limitations on peak broadening, they did not study the mass transfer kinetics in their phase system. Slow mass transfer and unsymmetrical peak profiles are associated with a heterogeneous distribution of adsorption energy (Guiochon et al., 1994). There are few publications discussing the kinetic properties of imprinted materials. Only their detailed study could clarify this issue.

Sajonz et al. (1998) measured the adsorption equilibrium isotherms and the mass transfer kinetics of L- and D-PA on a polymeric stationary phase imprinted with L-PA at four different temperatures, 313, 323, 333, and 343 K. This information was derived from experimental breakthrough curves measured in staircase frontal analysis. The equilibrium data were well accounted for by the Bi−Langmuir and the Freundlich isotherms but not by the simpler Langmuir isotherm. This suggested that the surfaces of the imprinted materials were energetically heterogeneous. The material was highly selective for the imprinted compound, L-PA, compared to its enantiomer. The lumped mass transfer rate coefficient ($k_{m,L}$) was derived from breakthrough curves by applying the transport model (Guiochon et al., 1994). The values of $k_{m,L}$ showed a positive concentration dependence, stronger for L-PA than for D-PA. A similar dependence was observed for $k_{m,L}$ in anion exchange chromatography of bovine serum albumin (BSA) (Guan-Sajonz et al., 1996; Sajonz et al., 1997) and for the mass transfer rate coefficient (k_m) in the enantiomeric separation of Tröger's base on microcrystalline cellulose triacetate (Seidel-Morgenstern et al., 1993; Rearden et al., 1998). Other publications report a concentration dependence of intraparticle diffusivity (Al-Duri and McKay, 1992), tracer diffusivity (Gibbs et al., 1991), axial dispersion (Lederer et al., 1990), effective diffusivity (Gallagher and Woodward, 1989), mutual diffusion coefficient (Marlowe and Jackson, 1990), and surface diffusion coefficients (Friedrich et al., 1988; Kapoor et al., 1989; Miyabe and Guiochon, 2000a). A concentration dependence of the mass transfer rate coefficients (k_m and $k_{m,L}$) and the diffusivities seems to be a general conclusion. It is expected that a more detailed analysis of the overall mass transfer rate parameter, $k_{m,L}$, in enantiomeric separations would provide new information on the kinetic properties of imprinted polymers.

Previous papers (Miyabe and Guiochon, 1999b,c, 2000b) advanced the quantitative analysis of the mass transfer characteristics of BSA in anion exchange chromatography (Miyabe and Guiochon, 1999b, 2000b) and of Tröger's base in its enantiomeric separation (Miyabe and Guiochon, 1999c). The contributions of four mass transport processes in a column, (1) axial dispersion, (2) fluid-to-particle mass transfer, (3) intraparticle diffusion, and (4)

adsorption/desorption, to $k_{m,L}$ or k_m were individually evaluated. In the anion exchange separation of BSA (Miyabe and Guiochon, 1999b, 2000b), surface diffusion played the major role in the kinetic properties of the mass transfer of BSA. The linear concentration dependence of $k_{m,L}$ seemed to originate from that of the surface diffusion coefficient (D_s). The positive concentration dependence of D_s could be interpreted by the heterogeneous surface model, suggesting that there was a wide distribution of the adsorption energy on the surface of anion exchangers. In the chiral separation of Tröger's base (Miyabe and Guiochon, 1999c), the mass transfer of the solute was significantly influenced by the kinetic properties of both intraparticle diffusion and adsorption/desorption. An attempt was also made to quantitatively interpret the thermodynamic properties of mass transfer in chiral separations.

Recently, interest shifted toward the optimization of the synthesis conditions of imprinted polymers and the selection of the mobile phase to improve the enantioselectivity of the chromatographic separations and the column efficiency (Sellergren, 1994). To evaluate the performance of imprinted materials and to develop a strategy for further improvements, detailed information on the mass transfer characteristics of chiral stationary phases must be made available. In a previous paper (Miyabe and Guiochon, 1999d), we reported on a brief analysis of the kinetic properties of an L-PA imprinted polymer at 313 K. The contribution of intraparticle diffusion to band broadening was shown to be more important than that of the other processes, i.e., axial dispersion, fluid-to-particle mass transfer, and adsorption/desorption. The positive concentration dependence of $k_{m,L}$ seemed to be explained by that of D_s. Although several models for surface diffusion were applied to interpret the concentration dependence of D_s, only the heterogeneous surface model gave a satisfactory result.

In this paper, we quantitatively reanalyze mass transfer kinetic data at 313−333 K reported in a previous paper (Sajonz et al., 1998), using the viscosity of acetonitrile/water solutions at these temperatures (Guiochon et al., 1994). Our goal was to clarify the kinetic properties of the polymeric stationary phase imprinted with L-PA in connection with phase equilibrium and thermodynamics data. The results of this study allow a comprehensive understanding of the mass transfer characteristics in this enantiomeric separation.

2. Theory

2.1. Adsorption Equilibrium. As shown previously (Sajonz et al., 1998), the experimental data on the adsorption equilibrium of L- and D-PA between a mixture of an aqueous buffer and acetonitrile, used as the mobile phase, and the polymeric imprinted stationary phase could be fitted as well to the Bi−Langmuir or the Freundlich isotherms:

$$q = \frac{a_1 C}{1 + b_1 C} + \frac{a_2 C}{1 + b_2 C} \quad (1)$$

$$q = a_F C^{1/n_F} \quad (2)$$

where C and q are the concentration of the solute in the mobile and the stationary phases, respectively, a_1, b_1, a_2, and b_2 are the numerical parameters of the Bi−Langmuir isotherm, and a_F and n_F are those of the Freundlich one. These parameters are independent of C.

2.2. Mass Transfer Kinetics. The lumped mass transfer rate coefficient ($k_{m,L}$) was determined from the experimental breakthrough curve obtained in frontal analysis, using the lumped kinetic model (Guiochon et al., 1994). The concentration dependence of $k_{m,L}$ was analyzed using equations derived for local linear chromatography (small relative height of the concentration steps).

2.2.1. General Kinetic Model in Chromatography. Band profiles in chromatography are completely described by the general kinetic model. This model includes the mass balance equations of the solute in the column and in the packing materials and kinetic equations describing the mass transfer of the solute between the three phases in the column, (1) the bulk mobile phase percolating through the bed of particles, (2) the mobile phase stagnant inside the porous particles, and (3) the stationary phase. The following HETP equation is derived from the first and second moments of the solution of the general kinetic model for chromatography (Guiochon et al., 1994):

$$H = \frac{2D_L}{u} +$$
$$2\left(\frac{k_1}{1+k_1}\right)^2\left[\frac{ud_p}{6Fk_f} + \frac{ud_p^2}{60FD_e} + \left(\frac{k_p}{1+k_p}\right)^2\frac{u}{FK_{ads}}\right] \quad (3)$$

with

$$k_1 = F(\epsilon_p + (1 - \epsilon_p)K_a) \quad (3a)$$

$$k_p = \frac{1 - \epsilon_p}{\epsilon_p}K_a \quad (3b)$$

where D_L is the axial dispersion coefficient, u is the average interstitial velocity of the mobile phase, d_p is the particle diameter, F is the phase ratio ($F = (1 - \epsilon_T)/\epsilon_T$, with ϵ_T the total column porosity), k_f is the external mass transfer coefficient, D_e is the intraparticle diffusivity, k_{ads} is the adsorption rate constant, ϵ_p is the internal porosity of the particle, and K_a is the adsorption equilibrium constant. Equation 3 includes several kinetic parameters, i.e., D_L, k_f, D_e, and k_{ads}. In this study, the following equations were used to estimate these kinetic parameters. The axial dispersion is usually assumed to consist of two mechanisms. One is molecular diffusion, and the other is fluid or eddy diffusion (Guiochon et al., 1994):

$$D_L = \gamma_1 D_m + \gamma_2 d_p u \quad (4)$$

where D_m is the molecular diffusivity. The contribution of molecular diffusion (the first term in the right-hand side (RHS) of eq 4) to D_L is relatively small compared to that of the second term, under the usual experimental conditions of liquid chromatography. The Wilson-Geankoplis equation was used to estimate k_f (Wilson and Geankoplis, 1966):

$$Sh = \frac{1.09}{\epsilon} Sc^{1/3} Re^{1/3} \quad (0.0015 < Re < 55) \quad (5)$$

where ϵ is the void fraction of the column (see definitions of Re, Sc, and Sh in the glossary of symbols). The value of D_m was estimated by the Wilke-Chang equation (Guiochon et al., 1994; Reid et al., 1977; Treybal, 1980):

$$D_{m,s} = 7.4 \times 10^{-8} \frac{(\alpha_{A,sv} M_{sv})^{1/2} T}{\eta_{sv} V_{b,s}^{0.6}} \tag{6}$$

where the subscripts s and sv denote the solute and the solvent, respectively, α_A is the association coefficient, M is the molecular weight, η is the viscosity, T is the absolute temperature, and V_b is the molar volume at normal boiling point. The contributions of pore and surface diffusions to intraparticle diffusion were separated by assuming the following relationship (Ruthven, 1984; Suzuki, 1990):

$$D_e = D_p + (1 - \epsilon_p) K_a D_s \tag{7}$$

where D_p and D_s are the pore diffusivity and the surface diffusion coefficient, respectively. The value of D_p was calculated by the following equation (Guiochon et al., 1994):

$$D_p = \left(\frac{\epsilon_p}{2 - \epsilon_p}\right)^2 D_m \tag{8}$$

2.2.2. Lumped Kinetic Model in Linear Chromatography.
The lumped kinetic model is effective for representing chromatographic behavior when one of the different mass transport processes in the column has a predominant influence on peak broadening (Guiochon et al., 1994):

$$\frac{\partial C}{\partial t} + F \frac{\partial C_s}{\partial t} + u \frac{\partial C}{\partial z} = D_L \frac{\partial^2 C}{\partial z^2} \tag{9}$$

$$\frac{\partial C_s}{\partial t} = k_m (C_s^* - C_s) \tag{10}$$

where C_s and C_s^* are the actual concentration of the solute and the solute concentration in the stationary phase in equilibrium with C, respectively, t is the time, z is the longitudinal distance along the column, and k_m is the lumped mass transfer rate coefficient. This coefficient represents the global effect of the contributions of all of the mass transfer resistances involved in the chromatographic system studied. The mass transfer rate is simply expressed as in eq 10 by using k_m on the assumption that the driving force of the mass transfer is the difference between C_s^* and C_s and the mass transfer rate is proportional to the driving force. The following HETP equation, valid for linear chromatography, was derived by van Deemter et al. (1956) from the analytical solution of eqs 9 and 10 proposed by Lapidus and Amundson (1952):

$$H = \frac{2D_L}{u} + 2\left(\frac{K'_0}{1 + K'_0}\right)^2 \frac{u}{K'_0 k_m} \tag{11}$$

where K'_0 is the retention factor at infinite dilution. Comparison of eqs 3 and 11 gives

$$\frac{F}{K'_0 k_m} = \frac{d_p}{6k_f} + \frac{d_p^2}{60 D_e} + \left(\frac{k_p}{1 + k_p}\right)^2 \frac{1}{k_{ads}} \tag{12}$$

Equation 12 indicates that the mass transfer rate coefficient in the solid film linear driving force model (k_m) is related to the three kinetic parameters, i.e., the external mass transfer coefficient (k_f), the intraparticle diffusivity (D_e), and the adsorption rate constant (k_{ads}),

and that the contributions due to the three mass transport processes are additive.

2.2.3. HETP Equation in Locally Linear Chromatography.
The following HETP equation was derived from the shock layer theory in frontal analysis under constant pattern behavior. It is valid in nonlinear chromatography, as long as the column efficiency is not very low (Guiochon et al., 1994):

$$H = \frac{2D_L}{u} + 2\left(\frac{K}{1 + K}\right)^2 \frac{u}{K k_m} \tag{13}$$

where K is the slope of the isotherm chord ($= F K_a = F(\Delta q / \Delta C)$). Equation 13 is same as eq 11, except that k'_0 was replaced by K. Equation 13 indicates that the contributions of axial dispersion and of the other mass transport processes are additive also in nonlinear chromatography, at least in frontal analysis and assuming the solid film linear driving force model. The only kinetic parameter, k_m, summarizes the contributions of all of the mass transfer processes in nonlinear frontal analysis, (1) fluid-to-particle mass transfer, (2) intraparticle diffusion, and (3) adsorption/desorption. As in linear chromatography, the following equation can be derived for locally linear chromatography:

$$\frac{F}{K k_m} = \frac{d_p}{6k_f} + \frac{d_p^2}{60 D_e} + \left(\frac{k_p}{1 + k_p}\right)^2 \frac{1}{k_{ads}} \tag{14}$$

Equation 14 is similar to eq 12 and represents the correlation between k_m and the three kinetic parameters, i.e., k_f, D_e, and k_{ads}.

2.2.4. Lumped Mass Transfer Rate Coefficient.
The lumped mass transfer rate coefficient ($k_{m,L}$) was determined from the experimental breakthrough curves and analyzed. The contribution of axial dispersion to band broadening is also lumped into $k_{m,L}$. The HETP can be written as a function of the Stanton number (St) as follows:

$$H = \frac{K}{(1 + K)^2} \frac{2L}{St} \tag{15}$$

with

$$St = \frac{k_{m,L} L}{u} \tag{15}$$

where L is the column length. Comparison of eqs 13 and 15 gives

$$\frac{1}{K k_{m,L}} = \left(\frac{1 + K}{K}\right)^2 \frac{D_L}{u^2} + \frac{1}{K k_m} \tag{16}$$

The following equation is derived from eqs 14 and 16:

$$\frac{F}{K k_{m,L}} = \left(\frac{1 + K}{K}\right)^2 \frac{F D_L}{u^2} + \frac{d_p}{6 k_f} + \frac{d_p^2}{60 D_e} + \left(\frac{k_p}{1 + k_p}\right)^2 \frac{1}{k_{ads}} \tag{17}$$

Equation 17 explains how the parameter $k_{m,L}$ correlates with the individual contributions of the four mass transport processes in the column. As described previously (Sajonz et al., 1998), $k_{m,L}$ depends on the concentration following an empirical relationship

$$k_{m,L} = k_{m,L}^0 C^m \tag{18}$$

where $k_{m,L}^0$ and m are numerical parameters, assumed to be independent of the solute concentration.

3. Experimental Section

We describe here only the information on the experimental conditions of the previous study (Sajonz et al., 1998) that is necessary to understand the analytical results of the present study. Other details can be found in the original paper (Sajonz et al., 1998).

3.1. Chromatographic Conditions. The structure and synthesis of the polymer imprinted with L-PA are described elsewhere (Sajonz et al., 1998). The polymeric stationary phase ($d_p = 25-35$ mm) was packed into a stainless steel column (10 cm × 0.46 cm). The mobile phase was a mixture of acetonitrile and an aqueous buffer solution (70:30, v/v). The buffer solution (pH 5.85) was prepared by dissolving orthophosphoric acid and sodium hydroxide in water. The hold-up volume of the column was 1.019 mL, measured by injecting acetonitrile (unretained). The total column porosity (ϵ_T) and the phase ratio (F) were 0.613 and 0.631, respectively. The column efficiency was 1060 and 880 plates for acetone (almost unretained) at 0.5 and 1 mL min^{-1}, respectively. Three sample solutions of each enantiomer (L- or D-PA) were prepared at 0.01, 0.1, and 1 mg mL^{-1}. The breakthrough curves were measured at a flow rate of 1 mL min^{-1}. The column temperature was successively 313, 323, and 333 K.

3.2. Procedures. After the column was washed and equilibrated, the breakthrough curves were recorded in an ascending staircase. Seven successive upward steps were performed, going from 0% to 5%, 5% to 10%, 10% to 20%, 20% to 40%, 40% to 60%, 60% to 80%, and 80% to 100% of the concentration of the sample solution. Because the concentration of the sample solutions were 0.01, 0.1, and 1 mg mL^{-1}, the range of the frontal analysis staircase was from 0 to 1 mg mL^{-1}. The height of a concentration step ranged from 5×10^{-4} to 0.2 mg mL^{-1}. All of the information on the phase equilibrium and the mass transfer kinetics was derived from these breakthrough curves. Each breakthrough curve gives one data point of the equilibrium isotherm and one value of $k_{m,L}$. The isotherm data were fitted to the Bi−Langmuir (eq 1) and the Freundlich models (eq 2). Breakthrough curves were calculated for each concentration step using the best values of the parameters of the equilibrium isotherm and different values of a constant $k_{m,L}$. The experimental breakthrough curves were compared to the calculated ones. The rate coefficient was determined as the value giving the best agreement between experimental and calculated breakthrough curves. It was assumed that $k_{m,L}$ was constant during each concentration step in the frontal analysis, corresponding to the average concentration of the concentration step.

4. Results and Discussion

In a previous paper, Sajonz et al. (1998) reported new data on the equilibrium thermodynamics and the mass transfer kinetics of L- and D-PA on a polymeric stationary phase imprinted with L-PA, at temperatures between 313 and 343 K. The numerical parameters characterizing the phase equilibrium and the mass transfer kinetics, i.e., a_1, b_1, a_2, b_2, a_F, n_F, $k_{m,L}^0$, and m, were determined from experimental breakthrough curves measured by staircase frontal analysis. They concluded that the adsorption equilibrium data were well accounted for by either the Bi−Langmuir or the Freundlich isotherms but not by the simpler Langmuir isotherm and that $k_{m,L}$ showed positive concentration dependence.
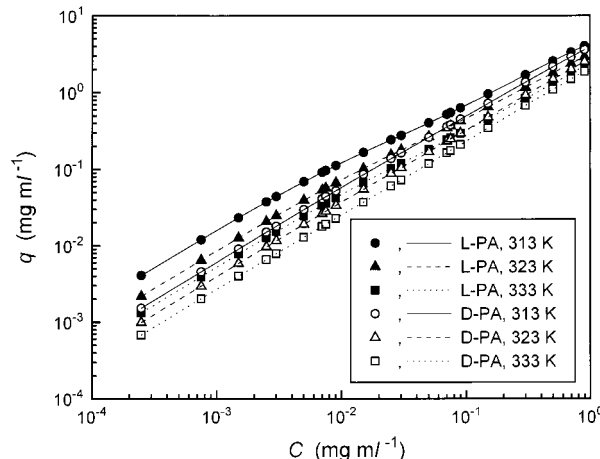
Figure 1. Best fit Bi−Langmuir isotherms of L- and D-PA on the polymeric stationary phase imprinted with L-PA.

In this paper, we report novel information concerning some characteristics of the mass transfer kinetics in the enantiomeric separation of L- and D-PA. This information was derived by reevaluating the experimental results reported previously (Sajonz et al., 1998). First, kinetic parameters were estimated by analyzing the concentration dependence of $k_{m,L}$. Second, the contributions of pore and surface diffusion to intraparticle diffusion were calculated, using the kinetic parameters previously estimated. Third, the concentration dependence of D_s was analyzed, taking into account the characteristics of the phase equilibrium and the thermodynamics. Finally, the characteristics of the adsorption and the mass transfer phenomena involved in the enantiomeric separation of L- and D-PA on the L-PA imprinted stationary phase were studied by taking into account the analytical results of the phase equilibrium, the mass transfer kinetics, and the thermodynamic properties.

4.1. Adsorption Equilibrium. Figure 1 shows the adsorption isotherm data of L- and D-PA (symbols; in almost all of the figures of this paper, the symbols represent experimental data and the lines represent the correlations of these data) on the polymeric imprinted stationary phase. Because of the wide range of solute concentrations sampled, the isotherm data are given as logarithmic plots. The amount of L-PA adsorbed is larger than that of D-PA at all temperatures and mobile phase concentrations. As indicated previously (Sajonz et al., 1998), the experimental data are well accounted for by either the Bi−Langmuir (eq 1) or the Freundlich isotherm (eq 2) and not by the simpler Langmuir isotherm. Table 1 shows the best values of the numerical parameters of the Bi−Langmuir and the Freundlich isotherms, i.e., a_1, b_1, a_2, b_2, a_F, and n_F. The lines in Figure 1 show the Bi−Langmuir equilibrium isotherms. Almost the same agreement could be observed with the Freundlich isotherm (not shown). The fact that the phase equilibrium is well described by the Bi−Langmuir equation does not imply the presence of only two types of interactions having different energies between the enantiomer molecules and the surface. There may be different types of adsorption sites and more complicated interactions on the heterogeneous surface of the imprinted stationary phase. A distribution of the adsorption energy can be predicted from the applicability of the Freundlich isotherm (Suzuki, 1990).The initial curvature of the equilibrium isotherm is relatively small because the values of nF listed in Table 1 are close to unity. When the height of the concentration step is small, the breakthrough curves are recorded under

Table 1. Parameters of the Equilibrium Isotherms and Mass Transfer Kinetics of L-PA and D-PA

	313 K		323 K		333 K	
	L-PA	D-PA	L-PA	D-PA	L-PA	D-PA
a_1	5.62	4.60	3.75	3.15	2.63	2.33
b_1 (mL mg^{-1})	0.35	0.20	0.24	0.16	0.15	0.14
a_2	10.9	1.50	5.02	0.82	2.69	0.40
b_2 (mL mg^{-1})	65.3	22.7	41.4	40.2	31.5	109
a_F (mg mL^{-1})	4.367	3.975	3.162	2.776	2.369	2.075
n_F	1.265	1.101	1.209	1.074	1.163	1.051
$k_{m,L}^0$ (s^{-1})	1.955	1.515	1.548	1.525	1.568	1.500
m	0.2582	0.1147	0.1860	0.1004	0.1714	0.0889

locally linear equilibrium conditions. In Figure 2a and 2b, the values of $\Delta q/\Delta C$ and $\delta q/\delta C$ at different solute concentrations are compared. As described earlier, the experimental breakthrough curves were measured in the ascending staircase frontal analysis mode, performing seven successive upward steps of the concentration of the sample solution in the eluent and using successively three sample solutions with different concentrations. A total of 21 breakthrough curves were recorded for each set of experimental conditions (sample component and temperature). The height of the concentration steps ranged from 5×10^{-4} to 0.2 mg mL^{-1}. The ratios $\Delta q/\Delta C$ in Figure 2a and 2b correspond to each concentration step. For instance, when a breakthrough curve was measured by changing the concentration of feed solution in the eluent from 80% to 100% (with a sample solution at 1 mg mL^{-1}), the initial concentration of the feed solution and the height of the concentration step were 0.8 and 0.2 mg mL^{-1}, respectively. The value of $\Delta q/\Delta C$ at C = 0.8 mg mL^{-1} was calculated by taking ΔC as 0.2 mg mL^{-1}. The values of q at the initial and final concentration of the eluent was calculated by using the Bi−Langmuir isotherm estimated in Figure 1. For the Bi−Langmuir isotherm, dq/dC was derived from the following equation (Guiochon et al., 1994):

$$\frac{dq}{dC} = \frac{a_1}{(1 + b_1 C)^2} + \frac{a_2}{(1 + b_2 C)^2} \qquad (19)$$

The solid ($\Delta q/\Delta C$) and dotted (dq/dC) lines are almost superimposed, irrespective of the temperature, in Figure 2a and 2b. Thus, the values of $k_{m,L}$ derived from the experimental breakthrough curves can be analyzed by assuming locally linear isotherm conditions.

4.2. Mass Transfer Rate Coefficient. Figure 3 shows plots of $k_{m,L}$ against C. The positive concentration dependence of $k_{m,L}$ was represented by eq 18 (Sajonz et al., 1998). Table 1 also lists the parameters $k_{m,L}^0$ and m. The lines in Figure 3 illustrate the correlations between $k_{m,L}$ and C calculated by eq 18. At low concentrations the values of $k_{m,L}$ are smaller for L-PA than for D-PA, irrespective of the temperature, a fact probably related to the high selectivity of the chiral stationary phase for L-PA. However, the difference between the values of $k_{m,L}$ for L- and D-PA decreases with increasing concentration. At high concentrations, almost the same values of $k_{m,L}$ are observed for L- and D-PA. This may be, at least partly, explained by an increase in the surface coverage at which these measurements were carried out. For example, the total saturation capacity ($q_s = (a_1/b_1) + (a_2/b_2)$) for L-PA at 313 K is 16.2 mg mL^{-1}. Measurements were carried out at mobile phase concentrations up to 1.0 mg mL^{-1}, for which q of L-PA at 313 K is ca. 4.3 mg mL^{-1}. The surface coverage ($q = q/q_s$) was about 27%. Similar calculations using the parameters listed in Table 1 indicate that q ranges from 0 to between 12% and 27%,
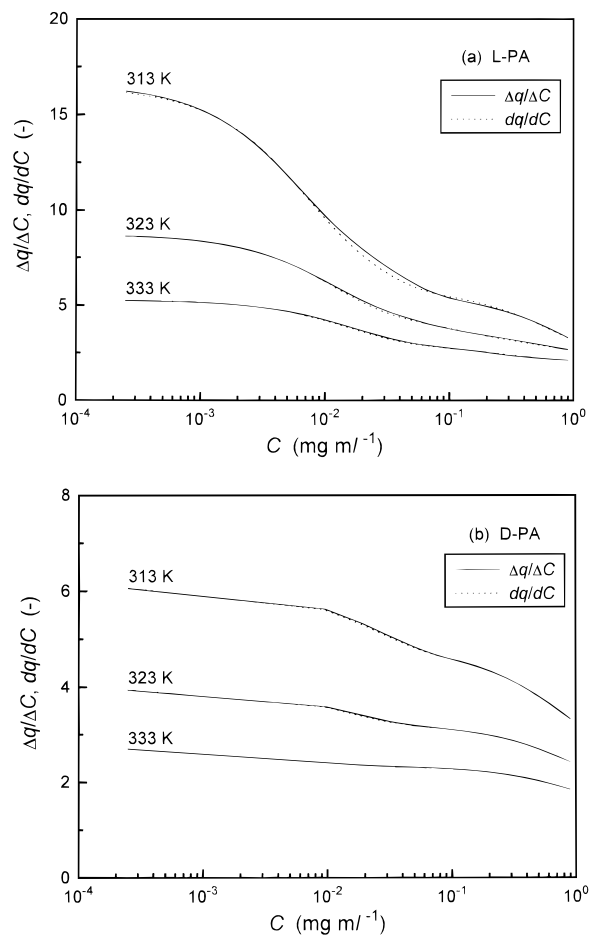
Figure 2. Comparison between the slope of the isotherm chord ($\Delta q/\Delta C$) and the tangent of the equilibrium isotherm (dq/dC). (a) L-PA, (b) D-PA.
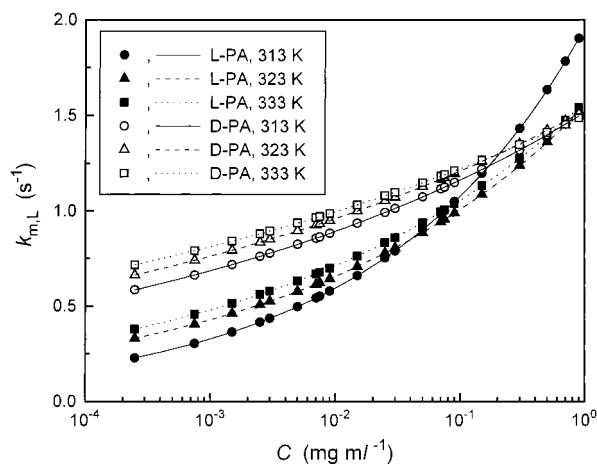
Figure 3. Dependence of $k_{m,L}$ on the concentration of the enantiomers.

depending on the temperature. The enantioselective adsorption sites are preferentially occupied by L-PA at low concentrations because the adsorption energy is higher. It is likely that most of these sites are already occupied at high concentrations. In Figure 1, although q of L-PA is about 2.5 times larger than that of D-PA at low concentrations, the relative difference between q for L- and for D-PA decreases also with increasing concentration. It seems that the results in Figures 1 and 3 are consistently interpreted by considering the concentration overload of the enantioselective sites for L-PA and their heterogeneous distribution.

The HETP (H) calculated by eqs 15 and 15a is between 0.024 and 0.20 cm for L-PA ($k_{m,L}$, 0.23–1.9 s^{-1}) and between 0.030 and 0.078 cm for D-PA ($k_{m,L}$, 0.59–1.5 s^{-1}) at 313 K, with u = 0.16 cm s^{-1}, L = 10 cm, and K = 5. These values are between 2 and 20 times larger than H obtained for an almost unretained compound (acetone), i.e., ca. 0.01 cm, suggesting that mass transfer processes inside the imprinted stationary phase (intraparticle diffusion and/or adsorption/desorption) influence significantly band broadening, more than axial dispersion and fluid-to-particle mass transfer. The kinetic properties of mass transfer inside the stationary phase must be clarified.

4.3. Estimation of Kinetic Parameters. Information on the kinetic parameters included in eq 17, i.e., D_L, k_f, D_e (D_p and D_s), and k_{ads}, was obtained as follows.

4.3.1. Estimation of D_L. First, D_L was estimated from the HETP values measured with an almost unretained compound (acetone). At K_a = 0, eq 3 is written as follows:

$$H = \frac{2D_L}{u} + 2\left(\frac{F\epsilon_p}{1 + F\epsilon_p}\right)^2\left[\frac{ud_p}{6Fk_f} + \frac{ud_p^2}{60FD_p}\right] \quad (20)$$

The following equation is derived from eqs 4 and 20 because the contribution of molecular diffusion to axial dispersion is negligibly small under the experimental conditions chosen:

$$H = 2\gamma_2 d_p + 2\left(\frac{F\epsilon_p}{1 + F\epsilon_p}\right)^2\left[\frac{ud_p}{6Fk_f} + \frac{ud_p^2}{60FD_p}\right] \quad (21)$$

The values of D_L/u (= $\gamma_2 d_p$) and FD_L/u^2 were calculated as 3.8×10^{-3} cm and 1.5×10^{-2} s, respectively, from the H values measured with acetone at flow rates of 0.5 and 1 mL min^{-1}, respectively. If K is assumed to be unity, the first term of the RHS of eq 17, $((1 + K)^2/K)(FD_L/u^2)$ becomes 6.0×10^{-2} s. Compared with the values of $F/(Kk_{m,L})$ obtained here, i.e., 0.15–0.51 s, that of $((1 + K)^2/K)(FD_L/u^2)$ is smaller by a factor of 2.5–8.6. So, the value of D_L/u was assumed to be constant, irrespective of the nature of the compounds (acetone or the enantiomers), of its concentration in the sample solutions, and of the temperature. This assumption has little influence on the conclusion of this study because of the small contribution of axial dispersion to the overall mass transfer resistance in the column.

The slope of the linear correlation between H and u provides information on k_f and D_p. These parameters can also be calculated using literature correlations (Guiochon et al., 1994; Ruthven, 1984; Suzuki, 1990). In this study, k_f and D_m were estimated from the Wilson-Geankoplis (Wilson and Geankoplis, 1966) and the Wilke-Chang equation (Guiochon et al., 1994; Reid et al., 1977; Treybal, 1980), respectively. The value of D_p for acetone was calculated with eq 8. The porosity of the packing material (ϵ_p) and the void fraction of the column (ϵ) were respectively estimated as 0.36 and 0.40 from the slope of the linear plot of H against u.

4.3.2. Estimation of k_f. Using eq 5, k_f was then estimated and included in the second term of the RHS of eq 17, $d_p/6k_f$. The value of D_m for the two enantiomers was estimated with eq 6. A value of 1.1×10^{-2} s at a flow rate of 1 mL min^{-1} was calculated for $d_p/(6k_f)$. It is between 14 and 46 times smaller than the experimental value of $F/(Kk_{m,L})$ and hence negligible in comparison with the other terms. The concentration dependences of D_m and k_f were not taken into account because it was shown experimentally that D_m varies little in the con-
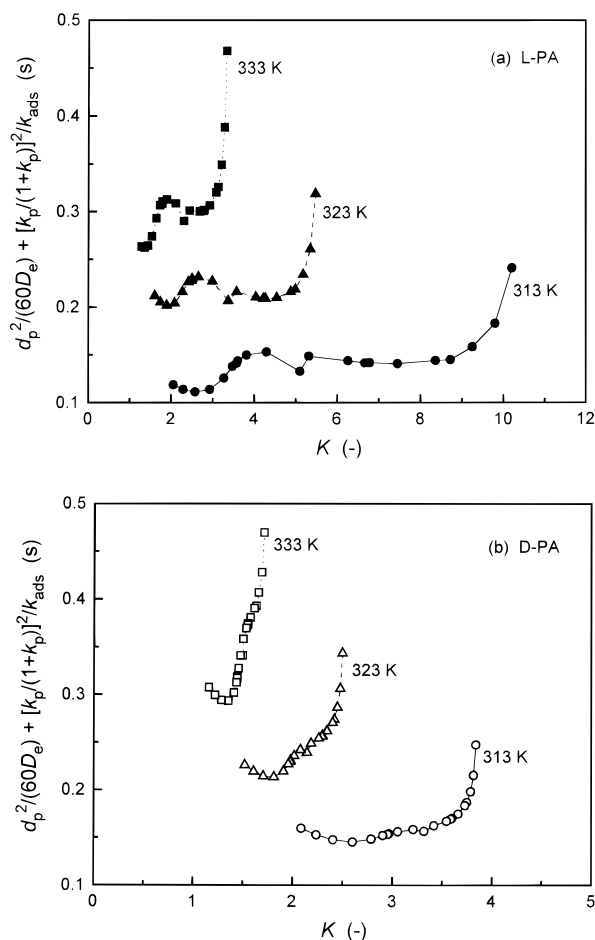
Figure 4. Correlation between $d_p^2/60D_e + [k_p/(1 + k_p)]^2/k_{ads}$ with K. (a) L-PA, (b) D-PA.

centration range 0–5% (Guiochon et al., 1994). This assumption has little influence on our results because of the small contribution of fluid-to-particle mass transfer to peak broadening.

4.3.3. Estimation of D_p. At this stage, the contributions of the first and second terms in the RHS of eq 17 are known since D_L and k_f are already estimated. Equations 7 and 17 suggest that the sum of the last two terms in the RHS of eq 17, i.e., $d_p^2/60D_e + (k_p/(1 + k_p))^2/k_{ads}$, becomes equal to $d_p^2/60D_p$ when K (and k_p) is zero. This sum is plotted against K in Figure 4. Although the data are somewhat scattered, the intercept at $K = 0$ seems to range between ca. 0.15 and 0.25 s at 313 K. From these values, D_p for L- and D-PA is estimated to be between 6×10^{-7} and 1×10^{-6} cm^2 s^{-1}. On the other hand, D_p is estimated to be 6.5×10^{-7} cm^2 s^{-1} at 313 K from eqs 6 and 8. Both estimates of D_p, from Figure 4 and from eqs 6 and 8 are close. A similar situation is observed at 323 K. The estimate of the intercept in Figure 4, at 323 K, is 0.2–0.3 s, suggesting that D_p is between 5×10^{-7} and 7.5×10^{-7} cm^2 s^{-1}, almost the same value as that given by eqs 6 and 8, i.e., 7.8×10^{-7} cm^2 s^{-1}. At 333 K, the intercept seems to be between 0.25 and 0.35 s, from which D_p is estimated at between 4.3×10^{-7} and 6×10^{-7} cm^2 s^{-1}, while eqs 6 and 8 provides $D_p = 9.4 \times 10^{-7}$ cm^2 s^{-1}. This time the agreement between the two estimates of D_p is not satisfactory.

Whereas the estimates of D_p derived from eqs 6 and 8 show an appropriate positive temperature dependence, those roughly estimated from the intercepts in Figure 4 exhibit an unreasonable slight decrease with increasing temperature. This might suggest that the actual mech-
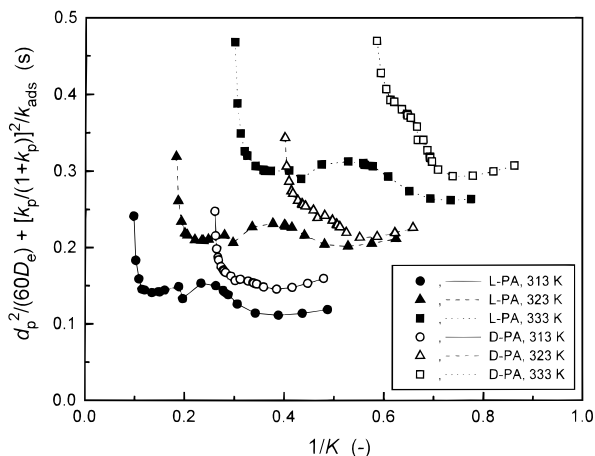
Figure 5. Correlation between $d_p^2/60D_e + [k_p/(1 + k_p)]^2/k_{ads}$ with $1/K$.

Figure 6. Plot of $[k_p/(1 + k_p)]^2$ against $1/K$.

anism of mass transfer inside the imprinted polymer is more complicated than implied by the kinetic model used in this study. As a consequence, the kinetic data at 313 and 323 K were analyzed further because it is likely that the values of D_p estimated at these temperatures are valid. In addition, the ratio D_p/D_m at 313 and 323 K was calculated to be ca. 0.048, using eqs 6 and 8. D_m is estimated from eq 6 to be 1.3×10^{-5} and 1.6×10^{-5} cm^2 s^{-1} at 313 and 323 K, respectively. This ratio D_p/D_m agrees well with previous observations that D_p is smaller than D_m by a factor between 3 and 30 for typical chromatographic packing materials (Guiochon et al., 1994). This also supports the conclusion that appropriate values of D_p were probably obtained at 313 and 323 K.

4.3.4. Estimation of k_{ads}. Equations 7 and 17 suggest that the sum $d_p^2/60D_e + (k_p/(1 + k_p))^2/k_{ads}$ tends toward $1/k_{ads}$ when K increases infinitely because the value of $(k_p/(1 + k_p))^2$ is unity at $K = \infty$. When the contribution of surface diffusion to intraparticle diffusion cannot be neglected compared to that of pore diffusion in eq 7, the third term in the RHS of eq 17, $d_p^2/60D_e$, might be neglected at $K = \infty$. Figure 5 shows the correlation between $d_p^2/60D_e + (k_p/(1 + k_p))^2/k_{ads}$ and $1/K$. Extremely rapid and important changes of the sum are observed at small values of $1/K$ in each case. In Figure 6, $(k_p/(1 + k_p))^2$ is plotted against $1/K$. $(k_p/(1 + k_p))^2$ decreases slowly with increasing $1/K$. The contribution of the fourth term in the RHS of eq 17, $(k_p/(1 + k_p))^2/k_{ads}$, to $k_{m,L}$ should vary as shown in Figure 6 because k_{ads} is assumed to be constant at each temperature. However, the profiles in Figures 5 and 6 are quite different, suggesting that the curves in Figure 5 cannot be explained by the kinetic properties of adsorption/desorption. It seems that the contribution of adsorption/desorption to the mass transfer kinetics in the imprinted stationary phase is smaller than that of intraparticle diffusion. A similar conclusion was reported by Sellergren et al. (1994, 1995). Therefore, it is unlikely that k_{ads} can be estimated by extrapolation of the plots in Figure 5.

As illustrated in Figure 6, the variation of $(k_p/(1 + k_p))^2$ at small values of $1/K$ is slow compared to that of $d_p^2/60D_e + (k_p/(1 + k_p))^2/k_{ads}$ in all cases shown in Figure 5. Because the contribution of $(k_p/(1 + k_p))^2/k_{ads}$ to $F/(Kk_{m,L})$ is small, as described earlier, the variation of $(k_p/(1 + k_p))^2/k_{ads}$ arising from that of $1/K$ may also be negligible compared to $F/(Kk_{m,L})$. In this case, the difference between the values of the sum $d_p^2/60D_e + (k_p/(1 + k_p))^2/k_{ads}$ at two different concentrations results from the difference of the two values of $1/D_e$ because the contribution of $(k_p/$
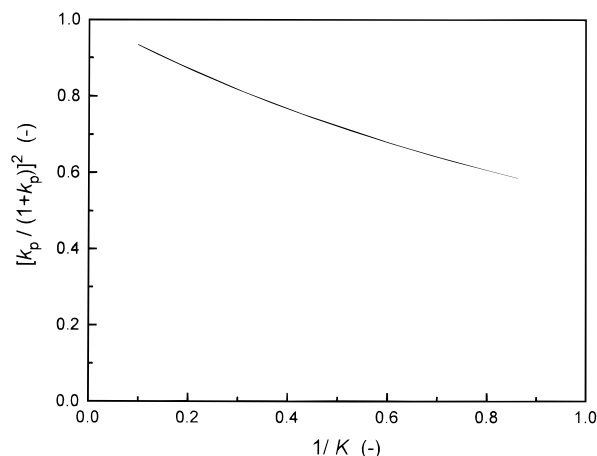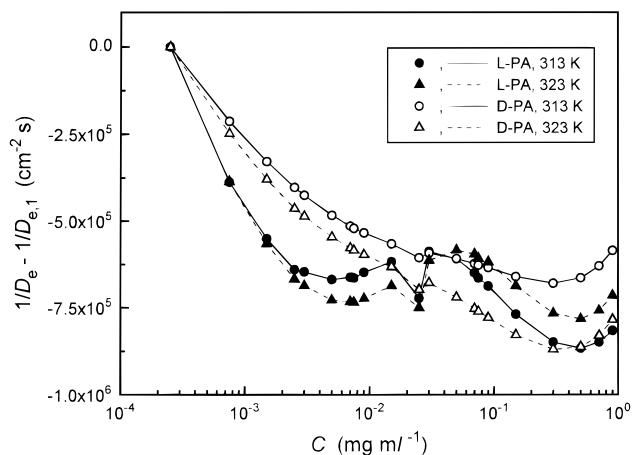
Figure 7. Concentration dependence of D_e. The value of D_e at the lowest concentration of the enantiomers ($D_{e,1}$) was taken as a reference.

$(1 + k_p))^2/k_{ads}$ to $F/(Kk_{m,L})$ is probably offset. In Figure 7, the difference between the values of $1/D_e$ at C and at the lowest average concentration ($C = 2.5 \times 10^{-4}$ mg mL^{-1}) denoted as $D_{e,1}$, is plotted against C. The difference is always negative since D_e tends to increase with increasing C. The concentration dependence of D_e is explained by that of D_s because D_m (namely, D_p) is assumed to be independent of C in this study. Thus, Figure 7 suggests that D_s increases with increasing C.

4.3.5. Estimation of D_s. The difference $(1/D_e - 1/D_{e,1})$ was calculated for the average concentration of each step in the assumption that the contribution of the change in $(k_p/(1 + k_p))^2/k_{ads}$ to that of $F/(Kk_{m,L})$ is relatively small. We could estimate D_s from the results in Figure 7 if we selected an appropriate value for $D_{e,1}$. For this purpose, we took D_p as $D_{e,1}$. The soundness of this assumption will be confirmed later. Figure 8 illustrates the concentration dependence of D_s at 313 and 323 K for both enantiomers. Overall, D_s increases with increasing concentration of each enantiomer. Since D_s was estimated by assuming $D_{e,1} = D_p$, the contribution of D_s to D_e is not completely neglected at the lowest concentration ($C = 2.5 \times 10^{-4}$ mg mL^{-1}). Yet, the conclusion that D_s exhibits a positive concentration dependence is unaffected. A similar positive concentration dependence of D_s was reported in reversed-phase liquid chromatography (Miyabe and Guiochon, 2000a), in anion exchange (Miyabe and Guiochon, 1999b, 2000b), and in other gas and liquid adsorption systems (Kapoor et al., 1989). In Figure 8, the value of D_s is between 1×10^{-8} and 1×10^{-6} cm^2 s^{-1}. The

Table 2. Surface and Lateral Diffusion Data in Previous Publications

solute	stationary phase	mobile phase	temp (K)	$D_s{}^a$ (cm^2 s^{-1})	D_m (cm^2 s^{-1})	D_m/D_s	reference
pyrene	C18	methanol/water (75/25, v/v)	b	2.5×10^{-7}	$5.5 \times 10^{-5\,c}$	220	Bogar et al., 1984
iodine	C1	methanol/water (50/50, v/v)	b	3.9×10^{-8}	$2.4 \times 10^{-5\,d}$	620	Wong and Harris, 1991
iodine	C1	methanol/water (75/25, v/v)	b	7.2×10^{-8}	$2.4 \times 10^{-5\,d}$	330	Wong and Harris, 1991
acridine orange	C18	water	293	1.3×10^{-7}	4.2×10^{-6}	32	Zulli et al., 1994
rubrene	C18	water	b	1.5×10^{-9}	$3.6 \times 10^{-6\,c}$	2400	Hansen and Harris, 1995
rubrene	C18	methanol/water (10/90, v/v)	b	2.1×10^{-9}	$3.0 \times 10^{-6\,c}$	1400	Hansen and Harris, 1995
rubrene	C18	methanol/water (20/80, v/v)	b	2.8×10^{-9}	$2.5 \times 10^{-6\,c}$	890	Hansen and Harris, 1995
BSA^e	poly(methyl-methacrylate)	aqueous buffer (pH 7.4)	310	1.2×10^{-9}	f	f	Tilton et al., 1990
BSA^e	poly(dimethyl-siloxane)	aqueous buffer (pH 7.4)	310	2.6×10^{-9}	f	f	Tilton et al., 1990
BSA	chitosan	aqueous buffer (pH 6.9)	298	4.7×10^{-10}	6.8×10^{-7}	1460	Yoshida et al., 1994
BSA	chitosan	aqueous buffer (pH 6.9)	298	2.4×10^{-9}	6.8×10^{-7}	290	Yoshida et al., 1994

^{a} D_s represents both surface and lateral diffusion coefficients. ^{b} No information about the temperature was indicated in the references. ^{c} D_m was estimated by assuming $T = 298$ K. ^{d} Data from the literature (*J. Phys. Chem.* **1991**, *95*, 4489–4495). ^{e} BSA was labeled with eosin isothiocyanate. ^{f} No calculations were made.
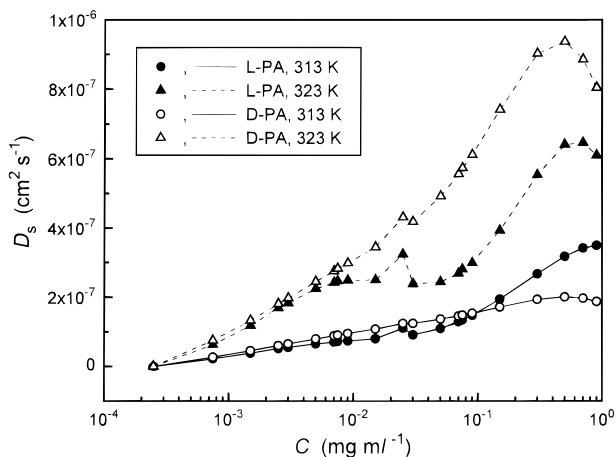
Figure 8. Concentration dependence of D_s at 313 and 323 K.

positive concentration dependence of D_s is verified irrespective of the D_s value at $C = 2.5 \times 10^{-4}$ mg mL^{-1}. However, the value of D_s at the lowest concentration influences those of D_s at higher concentrations. The validity of the values estimated for D_s at other concentrations will be confirmed later.

The value of D_s is influenced by the physical and chemical properties of the solutes and the stationary and the mobile phases in the separation system. However, no data on D_s were ever reported previously for L- and D-PA on an imprinted stationary phase. So, we discuss here some literature data on D_s for other systems. In a previous paper (Miyabe and Guiochon, 2000a), we reviewed surface diffusion data in reversed-phase liquid chromatography (RPLC) determined under various experimental conditions for different systems. Values of D_s between 1×10^{-7} and 1×10^{-5} cm^2 s^{-1} were reported. D_s was found to be a few orders of magnitude smaller than D_m (Miyabe and Guiochon, 1999a, 2000a). Other experimental data were also reported on surface and lateral diffusions in RPLC (Bogar et al., 1984; Hansen and Harris, 1995; Wong and Harris, 1991; Zulli et al., 1994) and in ion exchange separation of BSA (Tilton et al., 1990; Yoshida et al., 1994). However, despite the general conclusion that diffusivity varies with the temperature, no information was provided for the temperature condi-

tions in many reports. Table 2 summarizes the results previously published. A similar conclusion is reached for the correlation between D_s and D_m. In this work, the ratio D_s/D_m was found to be between 1/610 and 1/20 at 313 and 323 K, values comparable with the results in Table 2. The validity of the values of D_s estimated at 313 and 323 K in this study seems established.

4.4. Comparison of the Contribution of Pore and Surface Diffusions to Intraparticle Diffusion. The important differences between the profiles of the curves in Figures 5 and 6 suggest that intraparticle diffusion plays probably a more important role in the overall mass transfer than adsorption/desorption. The characteristics of the concentration dependence of D_e should be analyzed in more detail because the kinetic properties of $k_{m,L}$ seem to depend mostly on those of D_e. Figure 9a illustrates the contributions of pore and surface diffusion to intraparticle diffusion of L-PA at 313 K as a function of C. While D_p remains constant, D_e increases with increasing concentration because of the similar dependence of K_a and D_s, as described in eq 7. The difference between D_e (solid circle) and D_p (open circle) in Figure 9a is the contribution of surface diffusion (open triangle) to the mass transfer of L-PA through the particles of stationary phase. At low concentrations, the contribution of surface diffusion is relatively small. It tends to increase with increasing C, although there is some scatter. Figure 9b shows similar results for D-PA. Although K_a decreases, as indicated in Figures 2a and 2b, D_e and $(1 - \epsilon_p)K_aD_s$ increase with increasing C. This positive concentration dependence of D_e and $(1 - \epsilon_p)K_aD_s$ is due to that of D_s.

As shown in Figures 1 and 2, the adsorption equilibrium constant (K) of L-PA is 2–3 times larger than that of D-PA at low concentrations (around 1×10^{-3} mg mL^{-1}). Figure 3 shows that $k_{m,L}$ is about twice smaller for L-PA than for D-PA around $C = 10^{-3}$ mg mL^{-1}. These results demonstrate that the imprinted enantiomer, i.e., L-PA, is more strongly adsorbed on the stationary phase and that its mass transfer rate is lower than that of D-PA. As explained above, the contribution of D_e to the mass transfer kinetics in the case studied is predominant. By taking into account the values of K and $k_{m,L}$ as indicated in eq 17, it is possible to compare the values of D_e derived from Figure 9a and 9b for L- and D-PA, respectively. However, the important differences observed for the
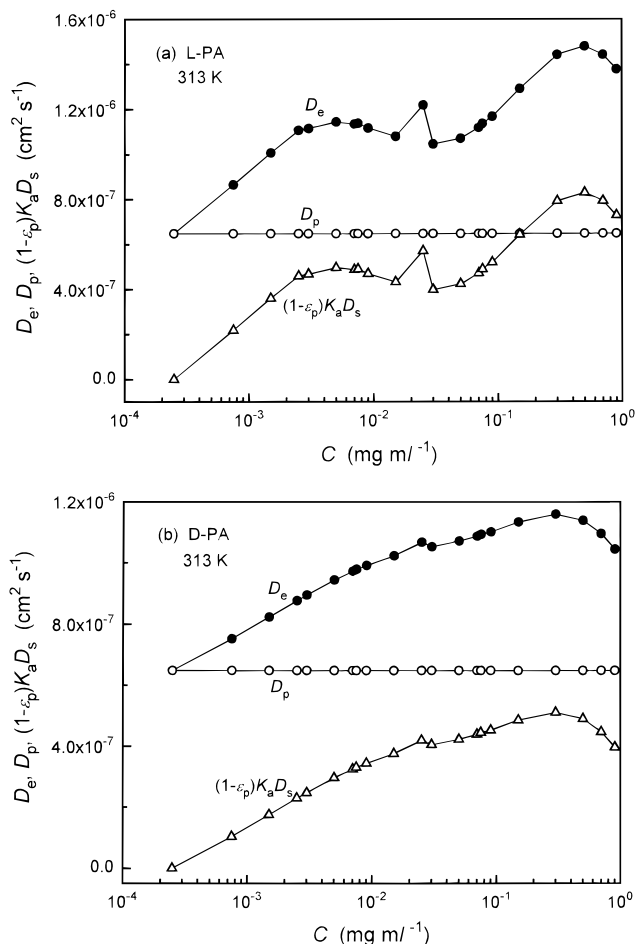
Figure 9. Comparison of the contribution of pore and surface diffusions to intraparticle diffusion. (a) L-PA, (b) D-PA.

adsorptivity and the mass transfer rate of L-PA and D-PA decrease with increasing concentration, as illustrated also in Figures 1−3. At low concentrations, the enantioselective adsorption sites are preferentially occupied by L-PA because their adsorption energy is high. At high concentrations, however, the enantioselective sites are saturated and the behavior of the stationary phase is controlled by that of the nonselective sites, which are the same for both enantiomers. For this reason, almost the same values of the amount adsorbed (q) and the rate coefficient ($k_{m,L}$) are observed for both enantiomers in the high concentration range (around 0.1−1 mg mL^{-1}) in Figures 1 and 3. Because the saturation capacity of the nonselective sites is much larger than that of the enantioselective adsorption sites, the inherent characteristics of the molecular imprinted phase are observed only at low concentration of the enantiomers.

In conclusion, the concentration dependence of $k_{m,L}$ illustrated in Figure 3 results from the positive concentration dependence of D_s because D_p is probably independent of C in the concentration range studied (between 0 and 0.3%). We showed that surface diffusion has a significant influence on the mass transfer kinetics of L- and D-PA on the imprinted polymer. Previously, we reported similarly important contributions of surface diffusion to the mass transfer kinetics in reversed-phase (Miyabe and Guiochon, 2000a) and in anion exchange chromatography (Miyabe and Guiochon, 1999b, 2000b). In RPLC with a C18-silica gel, the concentration dependence of D_s of p-tert-octylphenol was interpreted using the chemical potential driving force model (Miyabe and Guiochon, 2000a). In anion exchange chromatography of

BSA, the heterogeneous surface model was effective for accounting for the positive concentration dependence of D_s (Miyabe and Guiochon, 1999b, 2000b). The characteristic features of surface diffusion need to be analyzed in more detail for a better understanding of the mass transfer characteristics inside the imprinted stationary phase.

4.5. Explanation of Concentration Dependence of D_s. The characteristics of surface diffusion are usually studied by analyzing the dependence of D_s on both the temperature and the amount adsorbed. Various theories and models were proposed for this purpose (Kapoor et al., 1989). The temperature dependence of D_s is usually analyzed by the Arrhenius equation on the basis of the assumption that surface diffusion is an activated process:

$$D_s = D_{s0} \exp\left(\frac{-E_s}{RT}\right) \quad (22)$$

where D_{s0} is the frequency factor of surface diffusion, E_s is its activation energy, and R is the universal gas constant. Correlations between the thermodynamic properties of phase equilibrium and those of surface diffusion were studied to investigate surface diffusion mechanism from the viewpoint of thermodynamics. For example, an empirical parameter (a) was used to correlate E_s with the isosteric heat of adsorption (Q_{st}). The value of a is usually between 0 and 1 for surface diffusion:

$$E_s = \alpha(-Q_{st}) \quad (23)$$

Combination of eqs 22 and 23 gives the following equation, with which many experimental data on the temperature dependence of D_s were analyzed:

$$D_s = D_{s0} \exp\left[-\alpha\frac{(-Q_{st})}{RT}\right] \quad (24)$$

Several models were proposed to explain the concentration dependence of D_s (Kapoor et al., 1989), for example, (1) the hopping model, (2) the heterogeneous surface model, (3) the Fick's law model, and (4) the surface pressure driving force model. Previously, we showed that the concentration dependence of D_s at 313 K of L- and D-PA on the imprinted polymer could be explained by the heterogeneous surface diffusion model, assuming an exponential decay for the distribution of the adsorption energy on the surface of the stationary phase (Miyabe and Guiochon, 1999d).

In the heterogeneous surface model, the Freundlich isotherm can be derived on the assumption that Q_{st} is proportional to the logarithm of q (Suzuki, 1990):

$$-Q_{st,q} = -Q_{st,0} + \gamma(\ln q) \quad (25)$$

where $Q_{st,q}$ and $Q_{st,0}$ are the isosteric heat of adsorption for an amount adsorbed q and at zero surface coverage, respectively, and γ is the negative slope of the linear correlation between $-Q_{st}$ and $\ln q$. As described previously (Sajonz et al., 1998), the phase equilibrium can also be represented by the Freundlich equation. Combination of eqs 24 and 25 gives

$$D_s = D_{s0}\left[q \exp\left(\frac{-Q_{st,0}}{\gamma}\right)\right]^{\alpha n_F} \quad (26)$$

where n_F is the reciprocal of the exponent of the Freundlich isotherm, equal to the ratio $-\gamma/(RT)$. Equation 26 suggests a linear correlation between $\ln D_s$ and $\ln q$, with
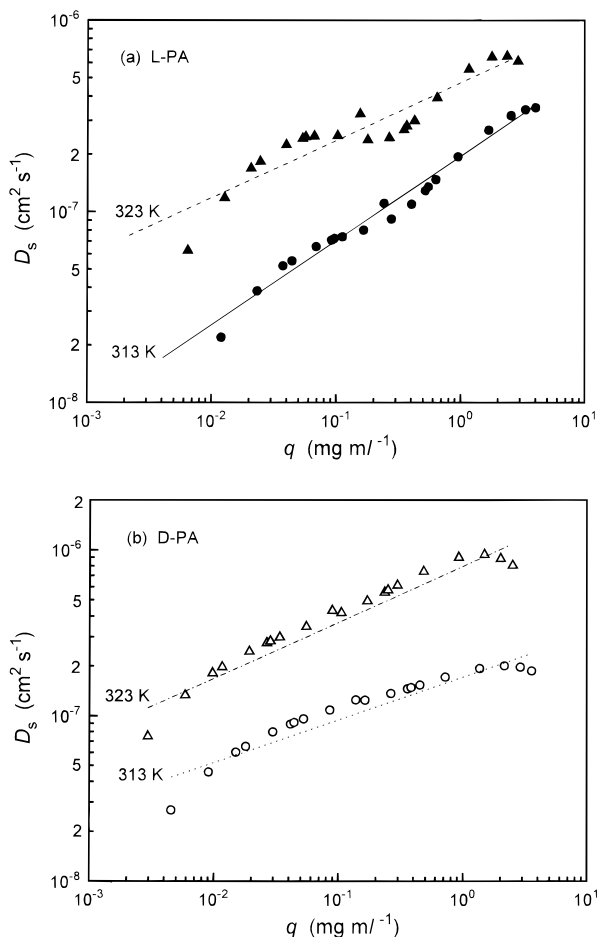
Figure 10. Interpretation of the concentration dependence of D_s by the heterogeneous surface model assuming the linear correlation between Q_{st} and the logarithm of q. (a) L-PA, (b) D-PA.

a slope an_F (Suzuki and Fujii, 1982). Figure 10a shows the plot between $\ln D_s$ and $\ln q$ for L-PA. The lines represent the best linear regression of the symbols, which are the values of D_s calculated for each amount adsorbed. Although the two plots exhibit somewhat winding profiles, linear correlations are likely in both cases, suggesting the applicability of eq 26 to explain the positive concentration dependence of D_s. The slopes of the straight lines are 0.44 (313 K) and 0.30 (323 K). The values of n_F are, respectively, 1.265 and 1.209 at these temperatures (Table 1). From these results, the average value of a is estimated at 0.30. Similar results observed for D-PA are shown in Figure 10b. The average value of a is estimated at 0.28 from the slopes of the straight lines, i.e., $an_F = 0.26$ (313 K) and 0.34 (323 K). This suggests that E_s is about 3.5 times smaller than $-Q_{st}$.

As described earlier, D_s was calculated by assuming that D_e for the lowest concentration of the enantiomers, $D_{e,1}$, was equal to D_p, i.e., that the contribution of surface diffusion to intraparticle diffusion was negligible at $C = 2.5 \times 10^{-4}$ mg mL^{-1}. We now discuss the validity of this assumption. The values of D_s of L- and D-PA at $C = 2.5 \times 10^{-4}$ mg mL^{-1} and 313 K are, respectively, estimated as 1.7×10^{-8} and 3.3×10^{-8} cm^2 s^{-1} from the linear correlations in Figure 10a and 10b. For L-PA, $(1 - \epsilon_p)K_aD_s$ and D_e are calculated as 1.7×10^{-7} and 8.2×10^{-7} cm^2 s^{-1}, respectively, by taking D_p as 6.5×10^{-7} cm^2 s^{-1}. This suggests that about 20% of the mass transfer flux of L-PA takes place by surface diffusion. Similar results are obtained for D-PA. The contribution of surface diffu-

sion to mass transfer in the stationary phase is estimated at 17% from the values of $(1 - \epsilon_p)K_aD_s$ and D_e, i.e., 1.3×10^{-7} and 7.8×10^{-7} cm^2 s^{-1}, respectively, for D-PA. These data indicate that the contribution of pore diffusion dominates intraparticle diffusion at low average concentrations. In addition, the uncertainty of D_s at the lowest concentration ($C = 2.5 \times 10^{-4}$ mg mL^{-1}) has probably little influence on the value of D_s at high concentrations, which support the validity of eq 26 as indicated in Figure 10a and 10b. The appropriateness of the procedure for estimating D_s is confirmed by the results in Figure 10a and 10b.

The adsorption equilibrium of L- and D-PA on the imprinted stationary phase was measured at four different temperatures, 313, 323, 333, and 343 K (Sajonz et al., 1998). The isosteric heat of adsorption, $Q_{st,q}$, was determined for various amounts adsorbed from the isosters corresponding to these amounts by the following equation:

$$\frac{d(\ln C^*)}{d(1/T)} = \frac{Q_{st,q}}{R} \tag{27}$$

where C^* is the mobile phase concentration in equilibrium with each amount adsorbed, estimated from the equilibrium isotherms at each temperature. Figures 11a and 11b show linear correlations between $\ln C^*$ and $1/T$ for L- and D-PA, respectively. The value of $Q_{st,q}$ was derived from the slope of these lines. Figure 12 shows the linear correlations between $Q_{st,q}$ and $\ln q$. As indicated previously (Sajonz et al., 1998), the adsorption equilibrium of the enantiomers could be modeled by the Bi—Langmuir or the Freundlich isotherms but not by the simpler Langmuir one, suggesting that the polymeric imprinted stationary phase had an energetically heterogeneous surface. The results in Figure 12 are consistent with this suggestion. The values of g are estimated as -4.3 (L-PA) and -2.0 (D-PA) from the slopes of the straight lines in Figure 12. For L-PA, a value of $1.60-1.64$ was calculated for $-\gamma/(RT)$ in the temperature range 313−323 K. As explained earlier, $-\gamma/(RT)$ should be equal to n_F. These values are similar to those of n_F for L-PA listed in Table 1, i.e., 1.265 (313 K) and 1.209 (323 K), although the agreement is only fair. Similar results are obtained for D-PA, with values of 0.77 and 0.74 for $-\gamma/(RT)$ at 313 and 323 K, respectively. The values of n_F for D-PA listed in Table 1 are 1.101 (313 K) and 1.074 (323 K). This suggest that the results of our analysis of the concentration dependence of D_s properly correspond to those relating to the phase equilibrium.

In summary, intrinsic characteristics of the polymer imprinted stationary phase are (1) the adsorption equilibrium can be represented by the Freundlich isotherm (Figure 1) (Sajonz et al., 1998); (2) $\ln D_s$ is almost proportional to $\ln q$ (Figures 10a and 10b); (3) $-Q_{st}$ decreases linearly with increasing $\ln q$ (Figure 12); and (4) the value of $-\gamma/(RT)$ calculated from the slope of the linear correlation between $-Q_{st}$ and $\ln q$ agrees approximately with n_F of the Freundlich isotherm. These results are self-consistent. Thus, we may conclude that the positive concentration dependence of D_s can be interpreted by the heterogeneous surface model and that E_s is about 30% of $-Q_{st}$. This paper shows how a kinetic study of the mass transfer in a stationary phase should take into account some characteristic features of the separation system, especially those of the phase equilibrium and its thermodynamics.
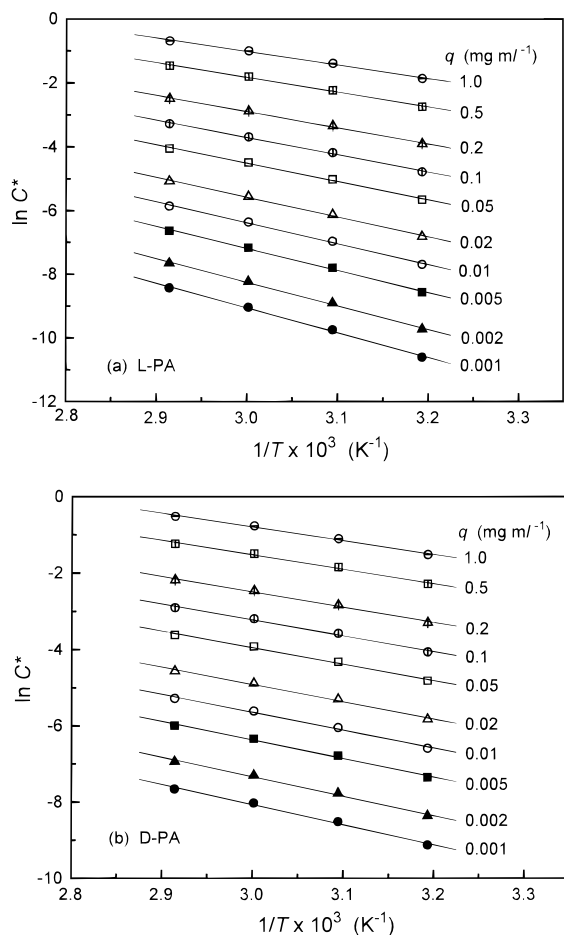
Figure 11. Plot between ln C^* and $1/T$ for determining $Q_{st,q}$. (a) L-PA, (b) D-PA.
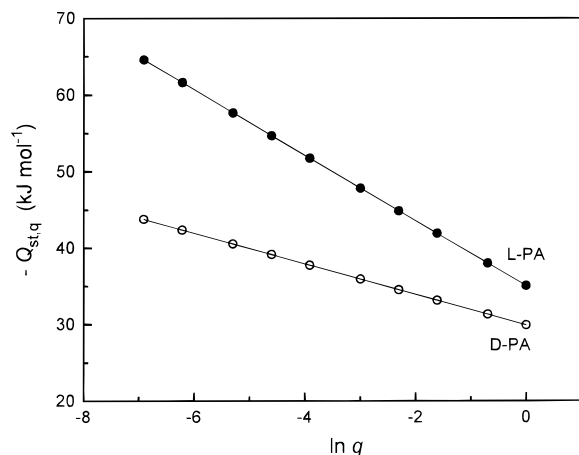
Figure 12. Linear correlations between $Q_{st,q}$ and ln q.

5. Conclusion

A quantitative analysis of the experimental data measured in the enantiomeric separation of L- and D-PA on a polymeric stationary phase imprinted with L-PA allowed the derivation of detailed information on mass transfer kinetics in this system. The kinetic parameters, i.e., D_e, D_p, and D_s, relating to the mass transfer inside the stationary phase were derived from the lumped rate coefficient, $k_{m,L}$. The contribution of intraparticle diffusion to overall mass transfer kinetics was shown to be larger than that of adsorption/desorption. The positive concentration dependence of $k_{m,L}$ resulted from that of D_s. The concentration dependence of D_s was interpreted using the

heterogeneous surface model. In conclusion, the distribution of adsorption energy on the heterogeneous surface of the imprinted stationary phase is probably an exponential decay function.

Notation

a_F	parameter of the Freundlich isotherm (eq 2) (mg mL^{-1})
a_1	parameter of the Bi−Langmuir isotherm (eq 1)
a_2	parameter of the Bi−Langmuir isotherm (eq 1)
b_1	parameter of the Bi−Langmuir isotherm (eq 1) (mL mg^{-1})
b_2	parameter of the Bi−Langmuir isotherm (eq 1) (mL mg^{-1})
C	concentration of the solute in the mobile phase (mg mL^{-1})
C^*	C in equilibrium with q (mg mL^{-1})
C_s	concentration of the solute adsorbed on the stationary phase (mg mL^{-1})
C_s^*	C_s in equilibrium with C (mg mL^{-1})
D_e	intraparticle diffusivity (cm^2 s^{-1})
$D_{e,1}$	D_e at the lowest concentration of the solute (cm^2 s^{-1})
D_L	axial dispersion coefficient (cm^2 s^{-1})
D_m	molecular diffusivity (cm^2 s^{-1})
d_p	particle diameter (cm)
D_p	pore diffusivity (cm^2 s^{-1})
D_s	surface diffusion coefficient (cm^2 s^{-1})
D_{s0}	frequency factor of surface diffusion (cm^2 s^{-1})
E_s	activation energy of surface diffusion (kJ mol^{-1})
F	phase ratio [= $(1 - \epsilon_T)/\epsilon_T$]
H	height equivalent to a theoretical plate (cm)
K	partition coefficient in nonlinear chromatography [= $FK_a = F(\Delta q/\Delta C)$]
K_a	adsorption equilibrium constant
k_{ads}	adsorption rate constant (s^{-1})
k_f	external mass transfer coefficient (cm s^{-1})
k_m	mass transfer rate coefficient representing the contributions of the fluid-to-particle mass transfer, the intraparticle diffusion, and the adsorption/desorption to band broadening (s^{-1})
$k_{m,L}$	lumped mass transfer rate coefficient representing the contributions of the axial dispersion, the fluid-to-particle mass transfer, the intraparticle diffusion, and the adsorption/desorption to band broadening (s^{-1})
$k_{m,L}^0$	parameter in eq 18 (s^{-1})
k_p	defined in eq 3b
k_0'	retention factor at infinite dilution
k_1	defined in eq 3a
L	column length (cm)
m	parameter in eq 18
M	molecular weight
n_F	reciprocal of the exponent of the Freundlich isotherm (eq 2)
q	concentration of the solute in the stationary phase (mg mL^{-1})
q_s	saturated amount adsorbed (mg mL^{-1})
Q_{st}	isosteric heat of adsorption (kJ mol^{-1})
$Q_{st,0}$	Q_{st} at zero surface coverage (kJ mol^{-1})
$Q_{st,q}$	Q_{st} at a given amount adsorbed (kJ mol^{-1})
R	gas constant (J mol^{-1} K^{-1})
Re	Reynolds number [= $d_p\epsilon_T u\rho/\eta$]
Sc	Schmidt number [= $\eta/(\rho D_m)$]
Sh	Sherwood number [= $k_f d_p/D_m$]

St	Stanton number $[= k_f L/u]$
t	time (s)
T	absolute temperature (K)
u	average interstitial velocity of the mobile phase (cm s^{-1})
V_b	molar volume at normal boiling point (cm^3 mol^{-1})
z	longitudinal distance along the column (cm)

Greek Symbols

α	ratio of E_s to $-Q_{st}$
α_A	association coefficient in eq 6
ϵ	void fraction of the column
ϵ_p	intraparticle porosity
ϵ_T	total porosity of the column
γ	parameter in eq 25
γ_1	parameter in eq 4
γ_2	parameter in eq 4
η	viscosity (Pa s)
θ	surface coverage
ρ	density (g cm^{-3})

Subscripts

s	unretained substance
sv	solvent

References and Notes

Al-Duri, B.; McKay, G. Pore Diffusion: Dependence of the Effective Diffusivity on the Initial Sorbate Concentration in Single and Multisolute Batch Adsorption Systems. *J. Chem. Technol. Biotechnol.* **1992**, *55*, 245.

Andersson, L. I. Application of Molecular Imprinting to the Development of Aqueous Buffer and Organic Solvent Based Radioligand Binding Assays for (*S*)-Propranolol. *Anal. Chem.* **1996**, *68*, 111.

Bogar, R. G.; Thomas, J. C.; Callis, J. B. Lateral Diffusion of Solutes Bound to the Alkyl Surface of C$_{18}$ Reversed-Phase Liquid Chromatographic Packings. *Anal. Chem.* **1984**, *56*, 1080.

Friedrich, M.; Seidel, A.; Gelbin, D. Kinetics of Adsorption of Phenol and Indole from Aqueous Solutions on Activated Carbons. *Chem. Eng. Process.* **1988**, *24*, 33.

Gallagher, W. H.; Woodward, C. K. The Concentration Dependence of the Diffusion Coefficient for Bovine Pancreatic Trypsin Inhibitor: A Dynamic Light Scattering Study of a Small Protein. *Biopolymers* **1989**, *28*, 2001.

Gibbs, S. J.; Chu, A. S.; Lightfoot, E. N.; Root, T. W. Ovalbumin Diffusion in Low Ionic Strength. *J. Phys. Chem.* **1991**, *95*, 467.

Guan-Sajonz, H.; Sajonz, P.; Zhong, G.; Guiochon, G. Study of the Mass Transfer Kinetics of BSA on a TSK-GEL DEAE–5PW Anion Exchanger in a Wide Concentration Range. *Biotechnol. Prog.* **1996**, *12*, 380.

Guiochon, G.; Golshan-Shirazi, S.; Katti, A. M. *Fundamentals of Preparative and Nonlinear Chromatography*; Academic Press: Boston, MA, 1994.

Hansen, R. L.; Harris, J. M. Lateral Diffusion of Molecules Partitioned into C-18 Ligands on Silica Surfaces. *Anal. Chem.* **1995**, *67*, 492.

Kapoor, A.; Yang, R. T.; Wong, C. Surface Diffusion. *Catal. Rev. Sci. Eng.* **1989**, *31*, 129.

Lapidus, L.; Amundson, N. R. Mathematics of Adsorption in Beds. VI. The Effect of Longitudinal Diffusion in Ion Exchange and Chromatographic Columns. *J. Phys. Chem.* **1952**, *56*, 984.

Lederer, K.; Amtmann, I.; Vijayakumar, S.; Billiani, J. Characterization of Poly(vinyl chloride) by Size Exclusion Chromatography. I. Concentration Dependence of Axial Dispersion Observed in Size Exclusion Chromatography Coupled with Light Scattering. *J. Liq. Chromatogr.* **1990**, *13*, 1849.

Marlowe, R. L.; Jackson, H. E. A Photon Correlation Study of the Concentration Dependence of Macromolecular Diffusion. *Spectrosc. Lett.* **1990**, *23*, 1203.

Miyabe, K.; Guiochon, G. Analysis of Surface Diffusion Phenomena in Reversed-Phase Liquid Chromatography. *Anal. Chem.* **1999a**, *71*, 889.

Miyabe, K.; Guiochon, G. Kinetic Study of the Concentration Dependence of the Mass Transfer Rate Coefficient in Anion Exchange Chromatography of Bovine Serum Albumin. *Biotechnol. Prog.* **1999b**, *15*, 740.

Miyabe, K.; Guiochon, G. Kinetic Study of the Mass Transfer of *S*-Tröger's Base in the Enantiomeric Separation System Using Cellulose Triacetate and Ethanol. *J. Chromatogr. A* **1999c**, *849*, 445.

Miyabe, K.; Guiochon, G. Kinetic Study of the Concentration Dependence of the Mass Transfer Rate Coefficient in Enantiomeric Separation on a Polymer Imprinted Stationary Phase. *Anal. Sci. (Jpn.)*, in press.

Miyabe, K.; Guiochon, G. Fundamental Interpretation of the Peak Profiles in Linear Reversed-Phase Liquid Chromatography. *Adv. Chromatogr.* **2000a**, *40*, 1.

Miyabe, K.; Guiochon, G. Kinetic Study of the Mass Transfer of Bovine Serum Albumin in Anion Exchange Chromatography. *J. Chromatogr. A* **2000b**, *866*, 147.

Rearden, P.; Sajonz, P.; Guiochon, G. Detailed Study of the Mass Transfer Kinetics of Tröger's Base on Cellulose Triacetate. *J. Chromatogr. A* **1998**, *813*, 1.

Reid, R. C.; Prausnitz, J. M.; Sherwood, T. K. *The Properties of Gases and Liquids*; McGraw-Hill: New York, 1977.

Ruthven, D. M. *Principles of Adsorption & Adsorption Processes*; John Wiley and Sons: New York, 1984.

Sajonz, P.; Guan-Sajonz, H.; Zhong, G.; Guiochon, G. Application of the Shock Layer Theory to the Determination of the Mass Transfer Rate Coefficient and Its Concentration Dependence for Proteins on Anion Exchange Columns. *Biotechnol. Prog.* **1997**, *13*, 170.

Sajonz, P.; Kele, M.; Zhong, G.; Sellergren, B.; Guiochon, G. Study of the Thermodynamics and Mass Transfer Kinetics of Two Enantiomers on a Polymeric Imprinted Stationary Phase. *J. Chromatogr. A* **1998**, *810*, 1.

Seidel-Morgenstern, A.; Jacobson, S. C.; Guiochon, G. Study of Band Broadening in Enantioselective Separations Using Microcrystalline Cellulose Triacetate. *J. Chromatogr.* **1993**, *637*, 19.

Sellergren, B. In *A Practical Approach to Chiral Separations by Liquid Chromatography*; Subramanian, G., Ed.; VCH: Weinheim, 1994; p 69.

Sellergren, B.; Lepisto, M.; Mosbach, K. Highly Enantioselective and Substrate-Selective Polymers Obtained by Molecular Imprinting Utilizing Noncovalent Interactions. NMR and Chromatographic Studies on the Nature of Recognition. *J. Am. Chem. Soc.* **1988**, *110*, 5853.

Sellergren, B.; Shea, K. J. Origin of Peak Asymmetry and the Effect of Temperature on Solute Retention in Enantiomer Separations on Imprinted Chiral Stationary Phases. *J. Chromatogr. A* **1995**, *690*, 29.

Shea, K. J.; Spivak, D. A.; Sellergren, B. Polymer Complements to Nucleotide Bases. Selective Binding of Adenine Derivatives to Imprinted Polymers. *J. Am. Chem. Soc.* **1993**, *115*, 3368.

Suzuki, M. *Adsorption Engineering*; Kodansha/Elsevier: Tokyo, 1990.

Suzuki, M.; Fujii, T. Concentration Dependence of Surface Diffusion Coefficient of Propionic Acid in Activated Carbon. *AIChE J.* **1982**, *28*, 380.

Tilton, R. D.; Robertson, C. R.; Gast, A. P. Lateral Diffusion of Bovine Serum Albumin Adsorbed at the Solid–Liquid Interface. *J. Colloid Interface Sci.* **1990**, *137*, 192.

Treybal, R. E. *Mass-Transfer Operations*; McGraw-Hill: New York, 1980.

van Deemter, J. J.; Zuiderweg, F. J.; Klinkenberg, A. Longitudinal Diffusion and Resistance to Mass Transfer as Causes of Nonideality in Chromatography. *Chem. Eng. Sci.* **1956**, *5*, 271.

Vlatakis, G.; Andersson, L. I.; Müller, R.; Mosbach, K. Drug Assay Using Antibody Mimics Made by Molecular Imprinting. *Nature* **1993**, *361*, 645.

Wilson, E. J.; Geankoplis, C. J. Liquid Mass Transfer at Very Low Reynolds Numbers in Packed Beds. *Ind. Eng. Chem. Fundam.* **1966**, *5*, 9.

Wong, A. L.; Harris, J. M. *J.* Surface Diffusion at the Liquid−Solid Interface: Quenching of Fluorescence from Pyrene Covalently Bound to Methylated Silica. *J. Phys. Chem.* **1991**, *95*, 5895.

Yoshida, H.; Yoshikawa, M.; Kataoka, T. Parallel Transport of BSA by Surface and Pore Diffusion in Strongly Basic Chitosan. *AIChE J.* **1994**, *40*, 2034.

Zulli, S. L.; Kovaleski, J. M.; Zhu, X. R.; Harris, J. M.; Wirth, M. J. Lateral Diffusion of an Adsorbate at a Chromatographic C$_{18}$/Water Interface. *Anal. Chem.* **1994**, *66*, 1708.